Enhanced lithium adsorption/diffusion and improved Li capacity on SnS_2 nanoribbons: A computational investigation

Kaixiong Tu, Fengyu Li, and Zhongfang Chen[a)]
Department of Chemistry, Institute of Functional Nanomaterials, University of Puerto Rico, San Juan, PR 00931, USA

(Received 6 July 2015; accepted 24 September 2015)

Density functional theory computations were performed to investigate the adsorption and diffusion properties of lithium (Li) on tin disulfides nanosheets and its derived nanoribbons (NRs), in comparison with SnS_2 bulk in 1T phase. The Li adsorption energies and migration barriers are comparable in SnS_2 bulk and bilayer, and Li adsorbed at the octahedral sites has the highest binding energy in both SnS_2 bulk and bilayer. Reducing the dimension of SnS_2 to monolayer significantly lowers the Li diffusion barrier while keeping a considerable binding energy, and lithium favors the hollow sites which corresponding to the octahedral sites in bulk phase. Due to the edge effect, SnS_2NRs gain an enhanced Li binding strength, increased Li mobility, and improved Li capacity. Thus, SnS_2 NRs are a promising candidate for anode materials of Li-ion batteries with a high power density and fast charge/discharge rates.

I. INTRODUCTION

Lithium-ion batteries (LIBs), as one of the most promising power source candidates for widespread consumer electronics and upcoming electric vehicles evolution, have gained great attention for past decades, due to their high energy density, light weight, fast charge and discharge efficiency, and long service life. To date, numerous materials, such as lithium alloys/multinary alloy,[1,2] graphitic/nongraphitic carbon,[3] transition metal dichalcogenides,[4–6] transition metal oxides,[7,8] polymers,[9] and their composites,[10] have been exploited as electrode materials of LIBs. Nevertheless, in spite of the extensive investigations, it remains a great challenge to further improve the capacity and cyclic life of the electrodes of LIBs.

To enhance the structural stability and electrical conductivity of electrode materials, major efforts have been made to reduce the size and dimensionality of the materials mentioned above in past decades,[11] owing to the quantum confinement effect and boundary effect.[12,13] Due to the high specific surface area and short lithium diffusion paths, nanomaterials displayed notably improved electrochemical performances.[14,15]

Recently, transition metal dicalcogenides have been demonstrated as very promising candidates for LIB electrodes on the basis of their unique chemical and physical properties, such as good conductivity, thermal stability, mechanical properties, and high charge–discharge cycles.[16] For instance, MoS_2 monolayer showed an excellent Li mobility and dynamic negative compressibility.[17] Furthermore, Li et al.'s theoretical work demonstrated that 1-D MoS_2 nanoribbons (NRs) were promising cathode materials for Li-ion batteries with a remarkably enhanced Li binding interaction and high Li mobility.[3]

Tin disulfide (SnS_2) is a typical post-transition metal dichalgenide material, which was first synthesized around 200 years ago[18] and has more than 70 polytypic structures.[19] While at ambient temperature, the thermodynamically stable polytope of SnS_2 (1T) consists of a trigonal lattice $P3m1$ (a = 3.65 Å; c = 5.90 Å)[20] with one layer per unit cell, where Sn(IV) ion is coordinated to six S ions in an octahedral environment.[21] Similar to graphite, these layers are held together by van der Waals (vdW) interactions. Such a unique structure endows SnS_2 as a key material for fundamental research and technological applications in opto-electronic devices,[22] catalysts,[23] sensors,[24] and electrochemical storage.[25]

Meanwhile, various morphologies of SnS_2 materials including nanoparticles,[26] nanoplates,[27] nanobelts,[28] nanowires,[29] and nanotubes[30] have been synthesized by different approaches and found to show efficient electrochemical performance,[31–35] since these nanostructures could better release the huge strain and stresses, buffer the volume change, and enhance lithiation/delithiation ability. For example, Luo et al.[25] demonstrated that SnS_2 nanoplates possess highly reversible capacity (~583 mA h/g) and excellent rate performance.

Very recently, Huang et al.[36] theoretically explored the Li adsorption and diffusion behavior on various SnS_2 nanostructures (bulk, bilayer, monolayer, zigzag NRs,

Contributing Editor: Jeremy T. Robinson
[a)]Address all correspondence to this author.
e-mail: zhongfangchen@gmail.com
DOI: 10.1557/jmr.2015.312

 © Materials Research Society 2015

https://doi.org/10.1557/jmr.2015.312 Published online by Cambridge University Press

and nanotubes) by means of density functional theory (DFT) computations with Vienna Ab-initio Simulation Package (VASP) code. Their results showed that Li adsorption in SnS_2 bulk and bilayer is stronger than the counterparts (monolayer, zigzag NRs, and nanotubes), but the diffusion is kinetically not as favorable as others. Besides, SnS_2 nanotubes gains Li binding strength, while sacrifices Li mobility and capacity when compared to SnS_2 monolayer.

Hence we further investigated the Li adsorption and diffusion properties on SnS_2 NRs in comparison with SnS_2 counterparts, to explore the potential of SnS_2 NRs for LIB anodes. Our computations show that SnS_2 NRs can provide improved Li binding strength, fast Li mobility, and high theoretical capacity, which indicates that SnS_2 NRs are a promising candidate of anode materials for LIBs with a high power density and fast charge–discharge rates.

II. COMPUTATIONAL METHODS

All the calculations were performed by using an all-electron method, as implemented in the DMol^3 code.[37,38] The generalized gradient approximation parameterization of Perdew–Burke–Ernzerhof (PBE)[39] of the exchange-correlation functional was adopted, together with the double numerical plus polarization basis set.[40] The convergence tolerance of the total energy and electron density was set to 10^{-6} a.u. for self-consistent field computations. We fixed the real-space global orbital cutoff radius as high as 5.1 Å in all computations to guarantee high-quality numerical results. The Brillouin zones of SnS_2 bulk, nanosheets, and NRs were represented by Monkhorst-Pack special k-point mesh of $4 \times 4 \times 4$, $4 \times 4 \times 1$ and $1 \times 1 \times 8$, respectively.

To investigate the Li adsorption and diffusion in the SnS_2 bulk/bilayers, a 3×3 supercell with one adsorbed Li atom was used, and the Grimme's PBE + $D2$ (D stands for dispersion) method,[41] which introduces dispersion correction by using an empirical potential of the form C_6R^{-6}, was adopted,[42] since the standard PBE functional cannot well describe the vdW interactions between individual layers, Li binding energies, and diffusion barriers in layered materials.[43] Furthermore, the transition states were located via the synchronous method with conjugated gradient (CG) refinements.[44] This method consists of repeated CG minimization after linear synchronous transit (LST) maximization, followed by repeated CG minimization next to quadratic synchronous transit (QST) maximizations until a transition state is located.

In our work, the Li binding energy, E_b(Li), is defined as $E_b(\mathrm{Li}) = E_{tot}(SnS_2) + E_{tot}(\mathrm{Li}) - E_{tot}(SnS_2\text{–Li})$, where $E_{tot}(SnS_2)$, E_{tot}(Li), and $E_{tot}(SnS_2\text{–Li})$ are the total energies of SnS_2 (bulk, bilayer, monolayer, or NRs), Li chemical potential, and Li-adsorbed SnS_2, respectively. According to this definition, the more positive the binding energy is, the higher exothermicity the lithiation in SnS_2 proceeds with.

III. RESULTS AND DISCUSSION

A. Li atom adsorption and diffusion in bulk SnS_2

We first studied the Li adsorption and diffusion behavior in a bulk phase of SnS_2. The optimized lattice constant c of SnS_2 bulk (5.91 Å) is in good consistence with experiment value (5.85–5.90 Å)[45] and previous theoretical works.[46] A $3 \times 3 \times 1$ supercell was used for SnS_2 bulk, which comprises 9 Sn atoms and 18 S atoms. There are two typical sites feasible for lithiation in SnS_2 bulk: (i) the octahedral (O_h) site, located in the center of nearest 6 S atoms from both of the triple layer [Fig. 1(a)]; and (ii) the tetrahedral (T_d) site, symmetrically located in the gap, where Li atom can bind to three S atoms from upper triple layer and a S atom from lower triple layer [Fig. 1(b)].

For the two examined adsorption sites, Li atom prefers to be adsorbed at the octahedral site with a binding energy of 1.85 eV, and the optimal mean distance between Li and surrounded S atoms is 2.58 Å. For lithiation at the tetrahedral site, it is also energetically favorable (with a binding energy of 1.39 eV); in this case, the lengths for upper and lower Li–S bonds are 2.24 and 2.35 Å, respectively.

In general, the electrochemical performance of an electrode is primarily determined by the Li mobility. Therefore it is necessary to study the diffusion path and barrier of Li in SnS_2 bulk. We considered the pathway that Li moving from an octahedral site to a nearby tetrahedral site, then to another octahedral site by adopting LST/QST method [Fig. 1(c)]. The computation showed a barrier of 0.69 eV, indicating that Li can migrate in bulk SnS_2. To further improve the Li mobility, we still need to reduce the diffusion barrier. And the SnS_2 nanosheets are expected to have a higher Li mobility than in SnS_2 bulk phase. The calculated binding energies, bond distances, and reaction barriers are consistence with recent study.[34]

B. Single Li atom adsorption and diffusion in bilayer and on monolayer

As a comparison, we also examined the Li adsorption and diffusion in both SnS_2 bilayer and SnS_2 monolayer, to check whether there is an improved Li mobility.

In SnS_2 bilayer, the interlayer distance is a little larger than that in bulk phase (5.95 Å versus 5.91 Å). Consequently, the newly formed Li–S bonds are also slightly longer than those in SnS_2 bulk (2.60 Å versus 2.58 Å). The octahedral site is more favorable for lithiation than the tetrahedral site (with a 1.8 and

https://doi.org/10.1557/jmr.2015.312 Published online by Cambridge University Press

1.32 eV binding energy, respectively), which is lower than that for corresponding site in SnS_2 bulk (1.85 and 1.32 eV, respectively). As expected, reducing the dimension from 3D bulk to 2D bilayer facilitates Li diffusion: SnS_2 bilayer showed a decreased diffusion barrier, which is 0.11 eV lower than that of SnS_2 bulk [Fig. 1(c)], when migrating between two neighboring O_h sites (0.58 eV versus 0.69 eV).

On SnS_2 monolayer, the hollow site (H), above the center of the hexagon [Fig. 2(a)], is more favorable for lithiation with a binding energy of 1.20 eV, slightly larger than that of the top site (T), directly above one Sn atom [Fig. 2(b)], with a binding energy of 1.07 eV. The other possibility for Li adsorption site, namely, atop of S atom, was also considered. But it is excluded since the Li atom spontaneously moves to nearby H site upon full relaxation.

We examined the Li diffusion routes on SnS_2 monolayer by migrating from an H site to another, while passing through a T site. The computed energy barrier is only 0.22 eV [Fig. 2(c)], which is smaller than that on MoS_2 monolayer (0.25 eV),[4] and the same as that of commercialized graphite anode (0.22 eV)[12] at the same theoretical level. Besides, it is dramatically lower than the diffusion barrier in SnS_2 bulk (0.69 eV) and SnS_2 bilayer (0.58 eV). This property was also found in TiS_2-related materials.[47]

We also estimated Li mobility (D) on the surface of SnS_2, as the Li mobility has a dominant effect on the rate performance of an electrode. By using the Arrhenius equation ($D \propto e^{-Ea/kT}$), it can be quantitatively estimated that Li mobility D in SnS_2 bilayer and on SnS_2 monolayer can be improved by a factor of 10^7 and 10^9, compared with that in SnS_2 bulk at room temperature, respectively.

C. Single Li atom adsorption and diffusion in 8-ZSnS$_2$NR

Even though the 2D SnS_2 nanosheets have much higher Li mobility, their decreased Li binding energies cannot make them ideal candidates for anode materials. Note that high Li binding energy is important to ensure the thermodynamic stability in anode materials. Though the recent theoretical work[31] showed that zigzag SnS_2 NRs have weak Li binding energies, the Li diffusion behaviors have not been addressed, and the armchair NRs have not been examined. Therefore, we further investigated the performance of Li adsorption and diffusion on

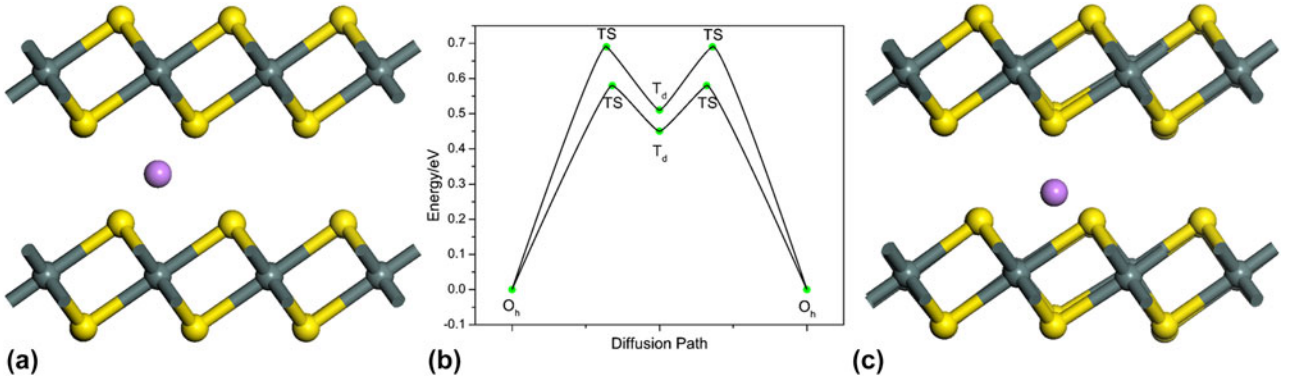


FIG. 1. Schematics of a Li atom adsorbed at the octahedral site (a) and tetrahedral site (c) of SnS_2 bulk in side view. (b) Lithium diffusion path (O_h–T_d–O_h) and barrier from an octahedral (O_h) site to another, passing through a tetrahedral (T_d) site in SnS_2 bulk, and bilayer. The gray, yellow and violet balls denote Sn, S, and Li atoms, respectively.

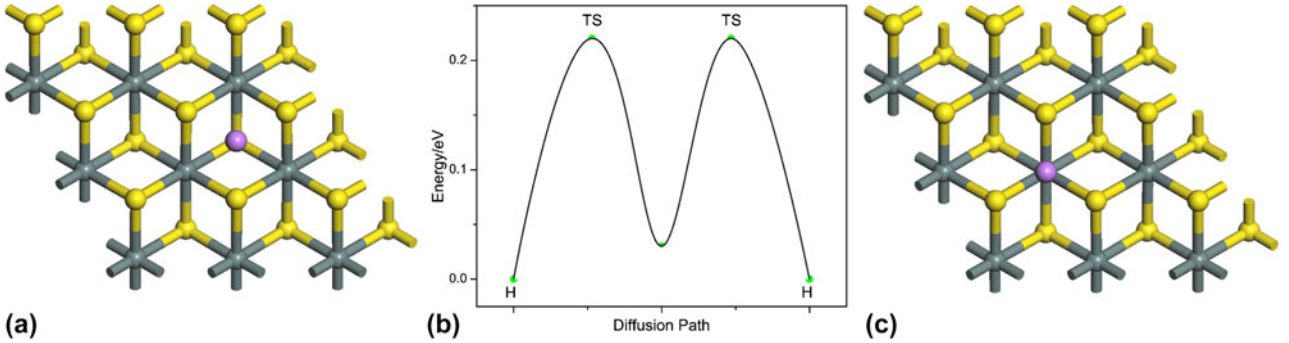


FIG. 2. Optimized geometries of a Li atom adsorbed at the H site (a) and T site (c) of SnS_2 monolayer. (b) Energy profile for Li diffusion on SnS_2 monolayer from an H site to another, passing through a T site.

https://doi.org/10.1557/jmr.2015.312 Published online by Cambridge University Press

1D NRs, since these behaviors may be affected via reducing the 2D materials into 1D nanostructure owing to the edge effect. Followed by the pronounced success in graphene and MoS_2 system[48] for improving Li binding energies, we expected that it is also possible to see the enhanced Li interactions with SnS_2NRs.

Similar to previous study,[49] two types of SnS_2NRs can be generated from the SnS_2 monolayer, namely, zigzag and armchair SnS_2NRs. Following the previous definition of graphene NRs, N_z-ZSnS_2NR (N_a-ASnS_2NR) is used to denote the zigzag-edged (armchair edged) SnS_2NR with a width of N_z zigzag chairs (N_a armchair chains). Here, we chose 8-ZSnS_2NR with the length of 25.53 Å and 15-ASnS_2NR with the length of 26.59 Å as the models for further study.

To evaluate the stabilities of SnS_2 NRs, we calculated the formation energy per atom (E_f) using the following definition: $E_f = (nE_{Sn} + mE_{S8}/8 - E_{SnS_2})/(n+m)$, where E_{Sn}, E_{S8}, and E_{SnS_2} represents the total energies of free Sn atom, crown-like S_8 molecular and SnS_2 NR, respectively, n (m) denotes the number of Sn (S) atoms in unit cell. Based on the definition, systems with larger E_f values (positive) are energetically more favorable. Our computations showed that 8-ZSnS_2NR and 15-ASnS_2NR have very close E_f values (1.54 and 1.53 eV/atom, respectively), which is in line to previous study[44]; therefore it seems very promising to synthesize the SnS_2 NRs in both armchair and zigzag forms.

For the electronic properties, SnS_2 NRs have smaller band gaps (1.67 eV for Z8SnS_2, 1.52 eV for A15SnS_2) than the SnS_2 monolayer (2.09 eV). The electronic property change due to the reduced dimensionality in NRs, or the edge effect, also occurs in other systems, such as in graphene,[12] MoS_2,[4] and MoO_3.[50]

Because of the low symmetry properties, there are many unique sites for Li adsorption available on the 8-ZSnS_2NR. In this study, we examined all the possible sites throughout the ribbon for lithiation on 8-ZSnS_2NR, containing 7 Hollow sites (H_1–H_7) and 8 Top sites (T_1–T_8) on the basal plane, and 4 sites on the side plane (S_1–S_4), as shown in Fig. 3(a).

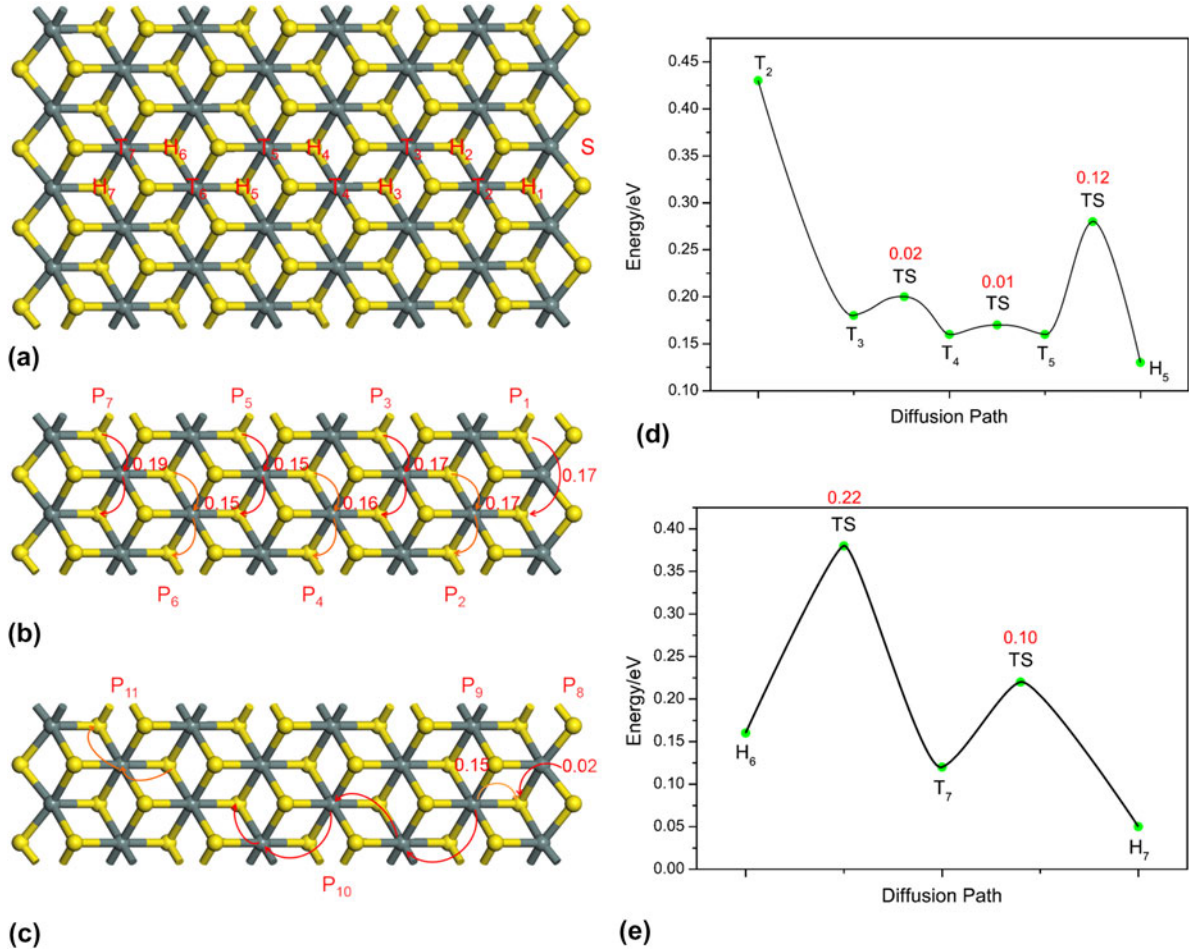


FIG. 3. Top view of the geometry of 8-ZSnS_2NR (a). All examined Li adsorption sites are marked with red characters. Li diffusion paths and energy barriers on 8-ZSnS_2NR along the axis direction (b). Li diffusion paths and energy barriers on 8-ZSnS_2NR along the transverse direction (c). Energy profiles for Li diffusion on P_{10} (d) and P_{11} (e) paths, respectively. The numbers indicate the energy barriers in electrovolts, and $E_b(H_1)$ is set as zero point energy.

https://doi.org/10.1557/jmr.2015.312 Published online by Cambridge University Press

The computed Li binding energies (E_b) and mean Li–S bond length ($L_{Li–S}$) for all the examined sites for 8-ZSnS_2NR and 15-ASnS_2NR are summarized in Table I. The T_1, T_8, are not local minimum sites for lithium adsorption. As upon relaxation, the Li atom on the T_1, and T_8 sites move to the near edge site H_1 and H_7, respectively. And S_2 and S_4 sites move to the corresponding S_1 and S_3 sites.

Similar to previous study,[31] the lithiation energies of all the considered binding sites on 8-ZSnS_2NR, except the high values at H_1 (E_b = 1.13 eV) and H_7 (E_b = 1.08 eV) sites, are in the range of 0.7–1.01 eV, which are slightly lower than those on the SnS_2 monolayer sheet (1.08 and 1.10 eV). On the basal plane, the H_i sites have a generally more favorable binding energy than the corresponding T_i sites, which is similar to the case on the SnS_2 monolayer. While, among all the considered adsorption sites, the 4-fold site H_1 near the edge region has the highest Li binding energy, followed by the edge hollow site H_7. The Li binding energies in the center sites are lower than that on the near-edge sites. At the edge site, the chemical environment of edge atoms is different from the central ones. For example, the edge S atoms only have two coordinated Sn atoms, while in the basal plane they are three coordinated; hence the edge S atoms are typically considered having dangling bond character. This special chemical environment may be the reason for the enhanced Li binding energy at the edge sites.

To examine whether dimension reduction affects the Li mobility, we further investigated the Li diffusion behavior along both the periodic direction [Fig. 3(b)] and transverse direction [Fig. 3(c)] of 8-ZSnS_2NR. Due to the asymmetrical structure property, various diffusion pathways have to be considered.

For Li diffusion routes along the periodic direction (as illustrated in Fig. 3), there are seven paths (p_i = H_i–T_i–H_i, i = 1–7) on the basal plane. The diffusion barriers decrease gradually from the edge to the center, with the magnitude between 0.15 and 0.19 eV, which are all smaller than those of similar diffusion route on SnS_2 monolayer (0.22 eV), and P_5 has the lowest diffusion barrier among the seven P_i routes (0.15 eV), implying the considerable edge effect.

For Li diffusing along transverse direction of 8-ZSnS_2NRs, there are four paths (P_8 = S–H_1, P_9 = H_1–T_2, P_{10} = T_2–T_3–T_4–T_5–H_5, P_{11} = H_6–T_7–H_7, see Fig. 1) on the basal plane. The energy barriers for Li migration of P_8–P_{10} are in the range of 0.02–0.13 eV, which have lower activation barriers than the periodic direction considered above, while P_{11} with a higher energy barrier of 0.22 eV. Obviously, Li prefers to diffuse along the transverse direction (P_8), which is

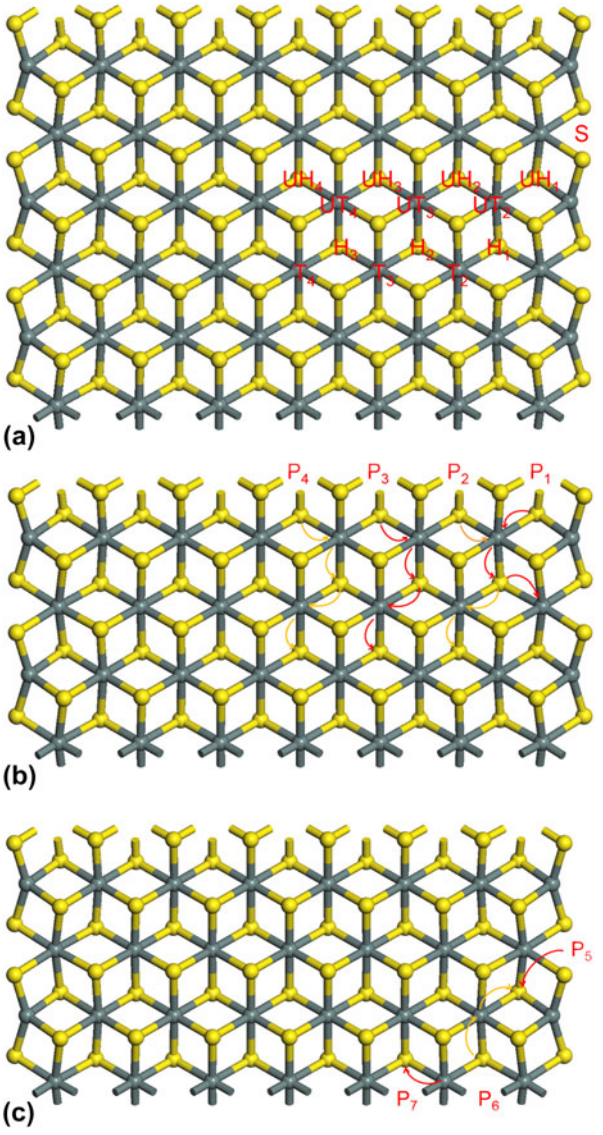


FIG. 4. Top view of geometry of 15-ASnS_2NR (a). All examined Li adsorption sites are marked with red characters. Li diffusion paths and energy barriers on 15-ASnS_2NR along the axis direction (b). Li diffusion paths and energy barriers on 8-ZSnS_2NR along the transverse direction (c). The numbers indicate the energy barriers in electrovolts and $E_b(UH_1)$ is set as zero point energy.

TABLE I. Computed Li binding energies (E_b), and mean Li–S bond length ($L_{Li–S}$) for all the examined Li adsorption sites of 8-ZSnS_2NR.

Site	H_1/S	H_2/T_2	H_3/T_3	H_4/T_4	H_5/T_5	H_6/T_6	H_7/T_7
E_b	1.13/0.78	0.93/0.70	0.99/0.95	1.00/0.97	1.00/0.97	0.97/0.95	1.08/1.01
$L_{Li–S}$	2.49/2.36	2.47/2.47	2.47/2.48	2.47/2.48	2.47/2.48	2.48/2.48	2.46/2.46

https://doi.org/10.1557/jmr.2015.312 Published online by Cambridge University Press

similar to the case of Li diffusion on the MoS_2 NRs, indicating certain percent of edge effect.

D. Single Li atom adsorption and diffusion in 15-ASnS$_2$NR

We also explored the lithiation behavior on 15-ASnS$_2$NR NR, since it has comparable stability as 8-ZSnS$_2$NR. More adsorption sites were involved, though it is symmetric, the structures of the two basal planes are different [Fig. 4(a)]. The Li binding strength on 15-ASnS$_2$NR (Table II) is slightly stronger than that on 8-ZSnS$_2$NR (Table I): the binding energies at hollow sites, top sites, upper hollow sites (UH), upper top sites (UT), and edge sites are in the range of 0.94–1.08, 0.99–1.03, 1.08–1.30, 1.00–1.02, and 1.20 eV, respectively. Among all the investigated lithiation sites, UH_1 has the largest E_b value (1.30 eV), which is much stronger than that of the energetically most favored site in monolayer. However, T_1/UT_1 site are not local minimum for lithiation, the Li atom on these sites move to the nearby H_1/UH_1 sites spontaneously upon relaxation.

Similar to the case on 8-ZSnS$_2$NRs, we examined all the possible Li diffusion routes along periodic direction (P_i = UH_i–UT_i–H_{i-1}–T_i–UH_i, i = 2–4; P_1 = UH_1–UT_2–H_1–UH_1) and that along transverse direction on the basal plane (P_5 = S–UH_1, P_6 = H_1–UT_2–UH_1, and P_7 = T_2–H_2).

For Li diffusion along the periodic directions [Fig. 4 (b)], the diffusion barrier is in the range of 0.17–0.48 eV [as shown in Figure 5], and P_4 has the lowest diffusion barrier (0.17 eV); moreover, the barrier of P_1 (0.48 eV), where the UH_1 has the strongest Li binding energy, is higher compared to the E_d value of similar diffusion pathway on SnS_2 monolayer (0.22 eV).

Along the transverse direction [Fig. 4(c)] on 15-ASnS$_2$NR, the Li diffusion barriers are in the range of 0.14 and 0.19 eV, while P_7 routes are relatively low (0.14 eV), which is lower than that corresponding route on 8-ZSnS$_2$NR (0.17 eV) and that on monolayer (0.22 eV), implying the considerable edge effect.

Apparently, it is likely for Li to diffuse along both the periodic direction and transverse direction on 15-ASnS$_2$NR, which is more complicated than the 8-ZSnS$_2$NR system. Similar to the situation of 8-ZSnS$_2$NR, Li diffusion barrier gradually decreases from edge to center in periodic direction, while the barrier is smaller near the edge in transverse direction. Similar behavior has also

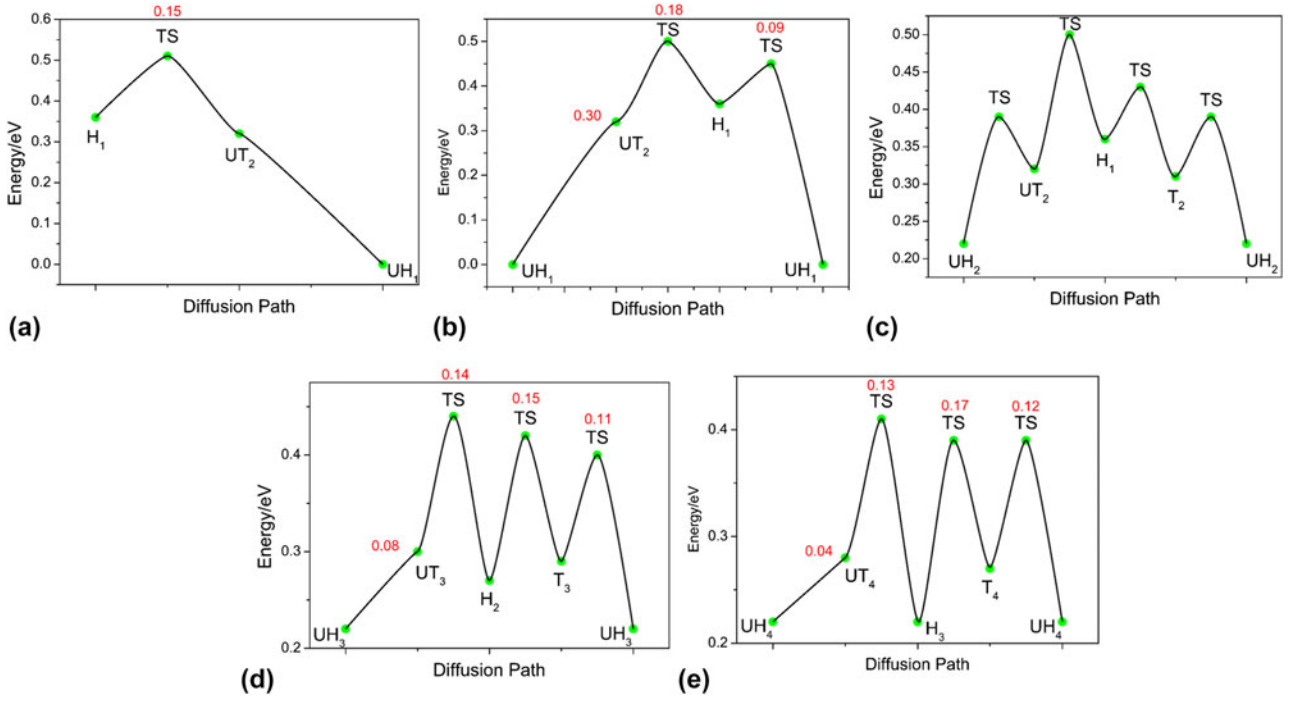


FIG. 5. Energy profiles for Li diffusion on P_6 (a) path along the transverse direction. Energy profiles for Li diffusion on P_1 (b), P_2 (c), P_3 (d), and P_4 (e) paths along the periodic direction, respectively. The numbers indicate the energy barriers in electrovolts.

TABLE II. Computed Li binding energies (E_b), and mean Li–S bond length ($L_{Li–S}$) for all the examined Li adsorption sites of 15-ASnS$_2$NR.

Site	H_1	H_2/T_2	H_3/T_3	T_4	UH_1/S	UH_2/UT_2	UH_3/UT_3	UH_4/UT_4
E_b	0.94	1.03/0.99	1.08/1.01	1.03	1.30/1.20	1.08/0.98	1.08/1.00	1.08/1.02
$L_{Li–S}$	2.61	2.63/2.49	2.63/2.49	2.49	2.45/2.3	2.48/2.60	2.48/2.62	2.48/2.64

https://doi.org/10.1557/jmr.2015.312 Published online by Cambridge University Press

been demonstrated in the graphene[12] and MoS_2 (Ref. 4) NR systems.

Finally, we calculated the Li storage capacity. The unit cell of 8-ZSnS_2NR and 15-ASnS_2NR can accumulate up to 20 and 36 Li atoms (to avoid phase separation, the distances of any adjacent Li atoms are all larger than that in Li metal), which correspond to the chemical stoichiometry of $SnS_2Li_{2.5}$ and $SnS_2Li_{2.4}$, respectively. Accordingly, their theoretical Li storage capacities are correspondingly 366 and 352 mA h/g, much larger than the counterparts of SnS_2 bulk (192 mA h/g), bilayer (228 mA h/g), and monolayer (293 mA h/g). Due to the edge and curvature effect, the Li storage capacity of SnS_2 NRs is expected to be higher than the nanotubes.

In the preceding section, we compared the Li adsorption, Li diffusion, and Li capacity in different SnS_2 nanostructures. The dimension reduction to 1D NRs, especially the armchair NRs, brings many advantages: the binding strength is enhanced as high as 0.2 eV compared to 2D monolayer; the Li diffusion barrier is lowered by up to 0.55 eV compare to bulk phase, correspondingly the mobility is improved by a factor of 10^9 according to the Arrhenius equation; the Li storage capacity is higher than the other structural morphologies. These exceptional features render SnS_2 NRs as promising LIB anode materials.

IV. CONCLUSIONS

In conclusion, we preformed DFT computations to investigate the Li adsorption and diffusion in SnS_2 bulk, bilayer, monolayer, and NRs. Comprehensive computations demonstrated that the Li mobility on SnS_2 monolayer can be remarkably increased compared with that in SnS_2 bulk. However, the Li binding energy of SnS_2 nanosheets is lower than that of SnS_2 bulk, which makes SnS_2 nanosheets not idea anode materials for LIB. While cutting SnS_2 nanosheets into SnS_2NRs can not only enhance the Li binding strength and Li capacity, but also preserve the high Li mobility. Therefore, SnS_2 NRs, particularly the armchair NRs, are promising as anode materials of Li-ion batteries with high performance. Our theoretical studies will hopefully inspire experimental studies on SnS_2NRs as anode materials.

ACKNOWLEDGMENTS

This work was supported by Department of Defense (Grant W911NF-12-1-0083) and NSF (Grant EPS-1002410).

REFERENCES

1. N. Liu, H. Wu, M.T. McDowell, Y. Yao, C.M. Wang, and Y. Cui: A yolk-shell design for stabilized and scalable Li-ion battery alloy anodes. *Nano Lett.* **12**(6), 3315 (2012).
2. H.C. Shin and M. Liu: Three-dimensional porous copper–tin alloy electrodes for rechargeable lithium batteries. *Adv. Funct. Mater.* **15**(4), 582–586 (2005).
3. T. Bhardwaj, A. Antic, B. Pavan, V. Barone, and B.D. Fahlman: Enhanced electrochemical lithium storage by graphene nanoribbons. *J. Am. Chem. Soc.* **132**(36), 12556 (2010).
4. Y. Li, D. Wu, Z. Zhou, C.R. Cabrera, and Z. Chen: Enhanced Li adsorption and diffusion on MoS_2 zigzag nanoribbons by edge effects: A computational study. *J. Phys. Chem. Lett.* **3**(16), 2221 (2012).
5. Y. Jing, Z. Zhou, C.R. Cabrera, and Z. Chen: Metallic VS_2 monolayer: A promising 2D anode material for lithium ion batteries. *J. Phys. Chem. C* **117**(48), 25409 (2013).
6. R. Bhandavat, L. David, and G. Singh: Synthesis of surface-functionalized WS_2 nanosheets and performance as Li-ion battery anodes. *J. Phys. Chem. Lett.* **3**(11), 1523 (2012).
7. C.K. Chan, H. Peng, R.D. Twesten, K. Jarausch, X.F. Zhang, and Y. Cui: Fast, completely reversible Li insertion in vanadium pentoxide nanoribbons. *Nano Lett.* **7**(2), 490 (2007).
8. L.Q. Mai, B. Hu, W. Chen, Y.Y. Qi, C.S. Lao, R.S. Yang, Y. Dai, and Z.L. Wang: Lithiated MoO_3 nanobelts with greatly improved performance for lithium batteries. *Adv. Mater.* **19**(21), 3712 (2007).
9. E-H. Kil, K-H. Choi, H-J. Ha, S. Xu, J.A. Rogers, M.R. Kim, Y-G. Lee, K.M. Kim, K.Y. Cho, and S-Y. Lee: Imprintable, bendable, and shape-conformable polymer electrolytes for versatile-shaped ;ithium-ion batteries. *Adv. Mater.* **25**(10), 1395 (2013).
10. K. Chang and W. Chen: L-cysteine-assisted synthesis of layered MoS_2/graphene composites with excellent electrochemical performances for lithium ion batteries. *ACS Nano* **5**(6), 4720–4728 (2011).
11. A.S. Arico, P. Bruce, B. Scrosati, J-M. Tarascon, and W. van Schalkwijk: Nanostructured materials for advanced energy conversion and storage devices. *Nat. Mater.* **4**(5), 366 (2005).
12. C. Uthaisar and V. Barone: Edge effects on the characteristics of Li diffusion in graphene. *Nano Lett.* **10**(8), 2838 (2010).
13. Q. Tang and Z. Zhou: Graphene-analogous low-dimensional materials. *Prog. Mater. Sci.* **58**(8), 1244 (2013).
14. M.E. Holtz, Y. Yu, D. Gunceler, J. Gao, R. Sundararaman, K.A. Schwarz, T.A. Arias, H.D. Abruña, and D.A. Muller: Nanoscale imaging of lithium ion distribution during in situ operation of battery electrode and electrolyte. *Nano Lett.* **14**(3), 1453 (2014).
15. Y. Jing, Z. Zhou, C.R. Cabrera, and Z. Chen: Graphene, inorganic graphene analogs and their composites for lithium ion batteries. *J. Mater. Chem. A* **2**(31), 12104 (2014).
16. H. Hwang, H. Kim, and J. Cho: MoS_2 nanoplates consisting of disordered graphene-like layers for high rate lithium battery anode materials. *Nano Lett.* **11**(11), 4826 (2011).
17. K.F. Mak, C. Lee, J. Hone, J. Shan, and T.F. Heinz: Atomically thin MoS_2: A new direct-gap semiconductor. *Phys. Rev. Lett.* **105**(13), 136805 (2010).
18. P. Woulfe:Experiments to show the Nature of Aurum Mosaicum: By Mr. Peter Woulfe, F.R.S. *Philos. Trans.* **61**, 114 (1771).
19. B. Palosz, W. Steurer, and H. Schulz: Refinement of SnS_2 polytypes 2H, 4H and 18R. *Acta Crystallogr., Sect. B* **46**(4), 449 (1990).
20. T. Jiang and G.A. Ozin: New directions in tin sulfide materials chemistry. *J. Mater. Chem.* **8**(5), 1099 (1998).
21. C.Y. Fong and M.L. Cohen: Electronic energy-band structure of SnS_2 and $SnSe_2$. *Phys. Rev. B* **5**(8), 3095 (1972).
22. S.R. Suryawanshi, S.S. Warule, N.S. Chaudhari, S.B. Ogale, and M.A. More: Photo-enhanced field emission characteristics of SnS_2 nanosheets. *AIP Conf. Proc.* **1591**, 342 (2014).
23. Y.C. Zhang, J. Li, M. Zhang, and D.D. Dionysiou: Size-tunable hydrothermal synthesis of SnS_2 nanocrystals with high performance in visible light-driven photocatalytic reduction of aqueous Cr(VI). *Environ. Sci. Technol.* **45**(21), 9324 (2011).
24. J. Li, Z. Yang, Y. Tang, Y. Zhang, and X. Hu: Carbon nanotubes-nanoflake-like SnS_2 nanocomposite for direct electrochemistry of glucose oxidase and glucose sensing. *Biosens. Bioelectron.* **41**, 698 (2013).

https://doi.org/10.1557/jmr.2015.312 Published online by Cambridge University Press

25. B. Luo, Y. Fang, B. Wang, J. Zhou, H. Song, and L. Zhi: Two dimensional graphene-SnS_2 hybrids with superior rate capability for lithium ion storage. *Energy Environ. Sci.* **5**(1), 5226 (2012).
26. S.Y. Hong, R. Popovitz-Biro, Y. Prior, and R. Tenne: Synthesis of SnS_2/SnS fullerene-like nanoparticles: A superlattice with polyhedral shape. *J. Am. Chem. Soc.* **125**(34), 10470 (2003).
27. J-w. Seo, J-t. Jang, S.-w. Park, C. Kim, B. Park, and J. Cheon: Two-dimensional SnS_2 nanoplates with extraordinary high discharge capacity for lithium ion batteries. *Adv. Mater.* **20**(22), 4269 (2008).
28. J. Yujie, Z. Hui, M. Xiangyang, X. Jin, and Y. Deren: Single-crystalline SnS_2 nano-belts fabricated by a novel hydrothermal method. *J. Phys.: Condens. Matter* **15**(44), L661 (2003).
29. Y-T. Lin, J-B. Shi, Y-C. Chen, C-J. Chen, and P-F. Wu: Synthesis and characterization of tin disulfide (SnS_2) nanowires. *Nanoscale Res. Lett.* **4**(7), 694 (2009).
30. D. Chen, G.Z. Shen, K.B. Tang, Y.K. Liu, and Y.T. Qian: Aligned SnS_2 nanotubes fabricated via a template-assisted solvent-relief process. *Appl. Phys. A* **77**(6), 747 (2003).
31. T. Momma, N. Shiraishi, A. Yoshizawa, T. Osaka, A. Gedanken, J. Zhu, and L. Sominski: SnS_2 anode for rechargeable lithium battery. *J. Power Sources* **97–98**, 198 (2001).
32. H. Mukaibo, A. Yoshizawa, T. Momma, and T. Osaka: Particle size and performance of SnS_2 anodes for rechargeable lithium batteries. *J. Power Sources* **119–121**, 60 (2003).
33. H.S. Kim, Y.H. Chung, S.H. Kang, and Y-E. Sung: Electrochemical behavior of carbon-coated SnS_2 for use as the anode in lithium-ion batteries. *Electrochim. Acta* **54**(13), 3606 (2009).
34. S. Liu, X. Yin, Q. Hao, M. Zhang, L. Li, L. Chen, Q. Li, Y. Wang, and T. Wang: Chemical bath deposition of SnS_2 nanowall arrays with improved electrochemical performance for lithium ion battery. *Mater. Lett.* **64**(21), 2350 (2010).
35. H. Zhong, G. Yang, H. Song, Q. Liao, H. Cui, and P. Shen, and C-X. Wang: Vertically aligned graphene-like SnS_2 ultrathin nanosheet arrays: Excellent energy storage, catalysis, photoconduction, and field-emitting performances. *J. Phys. Chem. C* **116**(16), 9319 (2012).
36. Y. Huang, C. Ling, X. Chen, D. Zhou, and S. Wang: SnS_2 nanotubes: A promising candidate for the anode material for lithium ion batteries. *RSC Adv.* **5**(41), 32505 (2015).
37. B. Delley: From molecules to solids with the DMol3 approach. *J. Chem. Phys.* **113**(18), 7756 (2000).
38. B. Delley: An all-electron numerical method for solving the local density functional for polyatomic molecules. *J. Chem. Phys.* **92**(1), 508 (1990).
39. J.P. Perdew, K. Burke, and M. Ernzerhof: Generalized gradient approximation made simple. *Phys. Rev. Lett.* **77**(18), 3865 (1996).
40. J.P. Perdew and Y. Wang: Accurate and simple analytic representation of the electron-gas correlation energy. *Phys. Rev. B* **45**(23), 13244 (1992).
41. S. Grimme: Semiempirical GGA-type density functional constructed with a long-range dispersion correction. *J. Comput. Chem.* **27**(15), 1787 (2006).
42. F. Ortmann, F. Bechstedt, and W.G. Schmidt: Semiempirical van der Waals correction to the density functional description of solids and molecular structures. *Phys. Rev. B* **73**(20), 205101 (2006).
43. J. Carrasco: Role of van der Waals forces in thermodynamics and kinetics of layered transition metal oxide electrodes: Alkali and alkaline-earth ion insertion into V_2O_5. *J. Phys. Chem. C* **118**(34), 19599 (2014).
44. N. Govind, M. Petersen, G. Fitzgerald, D. King-Smith, and J. Andzelm: A generalized synchronous transit method for transition state location. *Comput. Mater. Sci.* **28**(2), 250 (2003).
45. B. Palosz and E. Salje: Lattice parameters and spontaneous strain in AX_2 polytypes: CdI_2, PbI_2, SnS_2 and $SnSe_2$. *J. Appl. Cryst.* **22**(6), 622 (1989).
46. I. Lefebvre-Devos, J. Olivier-Fourcade, J.C. Jumas, and P. Lavela: Lithium insertion mechanism in SnS_2. *Phys. Rev. B* **61**(4), 3110–3116 (2000).
47. K. Tibbetts, C.R. Miranda, Y.S. Meng, and G. Ceder: An ab initio study of lithium diffusion in titanium disulfide nanotubes. *Chem. Mater.* **19**(22), 5302 (2007).
48. C. Uthaisar, V. Barone, and J.E. Peralta: Lithium adsorption on zigzag graphene nanoribbons. *J. Appl. Phys.* **106**(11), 113715 (2009).
49. L.Z. Li, H. Li, J. Zhou, J. Lu, R. Qin, Z.X. Gao, and W.N. Mei: Electronic structure and stability of ultranarrow single-layer SnS_2 nanaoribbons: A first-principles study. *J. Comput. Theor. Nanosci.* **7**(10), 2100 (2010).
50. F. Li, C.R. Cabrera, and Z. Chen: Theoretical design of MoO_3-based high-rate lithium ion battery electrodes: The effect of dimensionality reduction. *J. Mater. Chem. A* **2**(45), 19180 (2014).

https://doi.org/10.1557/jmr.2015.312 Published online by Cambridge University Press